First-principles study of high-pressure phase stability and superconductivity of Bi$_4$I$_4$

Shiyu Deng [1,2,3] Xianqi Song [1] Xuecheng Shao,[1] Quan Li [1,*] Yu Xie [1,†] Changfeng Chen [4,‡] and Yanming Ma [1]

[1]*State Key Laboratory of Superhard Materials, Key Laboratory of Automobile Materials of MOE, Department of Materials Science, and Innovation Center for Computational Physics Method and Software, Jilin University, Changchun 130012, China*
[2]*Department of Materials Science, ETH Zürich, CH-8092, Switzerland*
[3]*Cavendish Laboratory, Cambridge University, J.J. Thomson Ave, Cambridge CB3 0HE, United Kingdom*
[4]*Department of Physics and Astronomy, University of Nevada, Las Vegas, Nevada 89154, USA*

Bismuth iodide Bi$_4$I$_4$ exhibits intricate crystal structures and topological insulating states that are highly susceptible to influence by environments, making its physical properties highly tunable by external conditions. In this work, we study the evolution of structural and electronic properties of Bi$_4$I$_4$ at high pressure using an advanced structure search method in conjunction with first-principles calculations. Our results indicate that the most stable ambient-pressure monoclinic α-Bi$_4$I$_4$ phase in $C2/m$ symmetry transforms to a trigonal $P31c$ structure (ε-Bi$_4$I$_4$) at 8.4 GPa, then to a tetragonal $P4/mmm$ structure (ζ-Bi$_4$I$_4$) above 16.6 GPa. In contrast to the semiconducting nature of ambient-pressure Bi$_4$I$_4$, the two high-pressure phases are metallic, in agreement with reported electrical measurements. The ε-Bi$_4$I$_4$ phase exhibits distinct ionic states of I$^{\delta-}$ and (Bi$_4$I$_3$)$^{\delta+}$ ($\delta = 0.4123$ e), driven by a pressure-induced volume reduction. We show that both ε- and ζ-Bi$_4$I$_4$ are superconductors, and the emergence of pressure-induced superconductivity might be intimately linked to the underlying structural phase transitions.

I. INTRODUCTION

Topological insulators (TIs) exhibit interesting fundamental physical properties and hold great promise for device applications [1]. These materials behave like insulators in their interior regions but bear conducting states at surfaces [2,3]. Notable discoveries of TIs include two-dimensional (2D) TIs in graphene [2] and HgTe quantum wells [4,5], 3D TIs in Bi$_{1-x}$Sb$_x$ [6,7], and Weyl semimetal (WSM) states in TaAs [8]. A vast majority of TIs belongs to the family of so-called strong topological insulators (STIs), in contrast to weak topological insulators (WTIs), and such classifications are made according to the nature of the surface states, primarily in the degree of the anisotropy of these states [9,10]. Compared to STIs, WTIs are much less understood due to intrinsic complexities of such states of matter and difficulties of the corresponding experimental detections [11]. As such, theoretical investigations, which have successfully predicted many STIs may once again help shed light on the nature and material characters of WTIs.

Recently, quasi-one-dimensional bismuth iodide β-Bi$_4$I$_4$ with the space group $C2/m$ (No. 12) has attracted considerable attention due to its potential capacity to be a novel TI [12–14]. Bismuth solid is a semimetal with strong spin-orbit interactions. In addition, bismuth is abundant, nontoxic, nonradioactive in nature and is accessible to industrial and economical mass production [15]. All these factors suggest Bi-based materials are promising TI candidates for practical purposes. Moreover, due to their non-quantum-Hall-like

topological features, Bi-based topological materials hold advantage over conventional TIs in many respects: (1) their topological states can be protected even at room temperature; (2) they are highly resilient to disorder, as most of them appear in bulk semiconductors; and (3) they can be turned into superconductors or WSMs via alloying or uniaxial strain [16]. Recent density-functional theory (DFT) calculations [12,13] demonstrate that β-Bi$_4$I$_4$ can be a WTI with Z$_2$ indices (0;001). Further calculations within the GW (where G refers to the Green's function and W to the dynamically screened Coulomb interaction) scheme show that once the quasiparticle effect [17] is taken into consideration, β-Bi$_4$I$_4$ becomes an STI (1;110) [12], the electronic structure of which is in proximity of the WTI phase (0;001) and the trivial insulator phase (0;000). Further investigation is needed to better understand its structural and electronic properties. Compared with other Bi-based TI candidates, Bi$_4$I$_4$ is stoichiometric and favors synthesis at a high purity level and can crystallize into a large single crystal [18,19], making this material an ideal platform for further experimental investigations.

Bi$_4$I$_4$ belongs to the family of one-dimensional molecular fragments, which are held together by comparatively weak noncovalent interactions. Hence, it is expected that the structures and properties of Bi$_4$I$_4$ can be effectively modulated by uniaxial strain [13] or external pressure [20,21]. A pressure-induced topological phase transition has been supported by experimental evidence that indicates a rapid decrease of resistivity in β-Bi$_4$I$_4$ around 8.8 [20] ∼10 GPa [21]. At increasing pressures, superconductivity starts to emerge. There results raise several fundamental questions concerning the underlying crystal structures and physical properties, especially the possible coexistence of topological states with superconductivity, resulting in topological superconducting states [22,23].

*liquan777@jlu.edu.cn
†xieyu@jlu.edu.cn
‡chen@physics.unlv.edu

Subsequent x-ray diffraction measurements together with an energy dispersive spectrometer analysis suggest that a new Bi-I phase is formed at high pressure, and this phase does not match any of previously known Bi-I compounds [21]. Determining the high-pressure structures is crucial to further study and understanding of fundamental properties of Bi_4I_4. To this end, we have systematically investigated the evolution of structural and electronic properties of Bi_4I_4 at high pressures. At ambient pressure, Bi_4I_4 crystallizes into a monoclinic phase with a space group of $C2/m$ and exhibits three structural forms (α-, β-, and γ-Bi_4I_4) [18]. Among them, α- and β-Bi_4I_4 exist at ambient temperature, while γ-Bi_4I_4 is only stable above 564 K and can easily decompose into BiI_3 and a lower iodide at 585 K. Hence, in the following sections, we will focus on α-Bi_4I_4 and β-Bi_4I_4 when referring to the previously reported equilibrium structure of $C2/m$ Bi_4I_4. DFT calculations are performed to determine the stable and metastable structures of Bi_4I_4 under various pressures. The results show that two new phases ($P31c$ and $P4/mmm$) turn up as pressure increases up to 40 GPa. The structural and electronic properties of the newly discovered phases differ considerably from the known α and β phases. Our results show that both phases are superconductive by an electron-phonon coupling (EPC) mechanism. Interestingly, the phase transition points well match the property-change points, providing a possibility to link the structural and superconducting phase transitions to a common underlying mechanism.

II. CALCULATIONAL METHODS

To determine the thermodynamically stable structures of Bi_4I_4 at various pressures, we carried out a systematic structure search utilizing a global minimization of free-energy surfaces based on the crystal structure analysis by particle swarm optimization (CALYPSO) [24–26] methodology in conjunction with first-principles energetic calculations. The advantage of this methodology is that it can effectively predict stable and metastable structures with only the knowledge of the chemical composition at given external conditions (e.g., pressure) [27–31]. The underlying *ab initio* energetic and electronic calculations were performed within the framework of DFT as implemented in the Vienna *ab initio* simulation package (VASP) code [32]. The generalized gradient approximation within the framework of Perdew-Burke-Ernzerhof [33] was used for the exchange-correlation functional. The electron-ion interaction was described by applying the projector augmented-wave method [34] with $5s^2 5p^5$ and $6s^2 6p^3$ treated as valence electrons for I and Bi atoms, respectively. To ensure that all the enthalpy calculations were well converged, the cutoff energy for the expansion of the wave-function into plane waves was set at 350 eV, and fine Monkhorst-Pack [35] k meshes were chosen to be $3\times9\times4$, $5\times5\times6$, and $11\times11\times4$ for $C2/m$, $P31c$, and $P4/mmm$ Bi_4I_4, respectively. The van der Waals interaction was considered using Grimme's approach (DFT-D2) [36]. Phonon dispersions were calculated to investigate lattice stability using the supercell approach as implemented in phonopy code [37], using forces obtained by the Hellmann-Feynman theorem calculated from the optimized $2\times2\times2$, $2\times2\times2$, and $3\times3\times2$ supercells for Bi_4I_4 with the space groups of $C2/m$, $P31c$, and
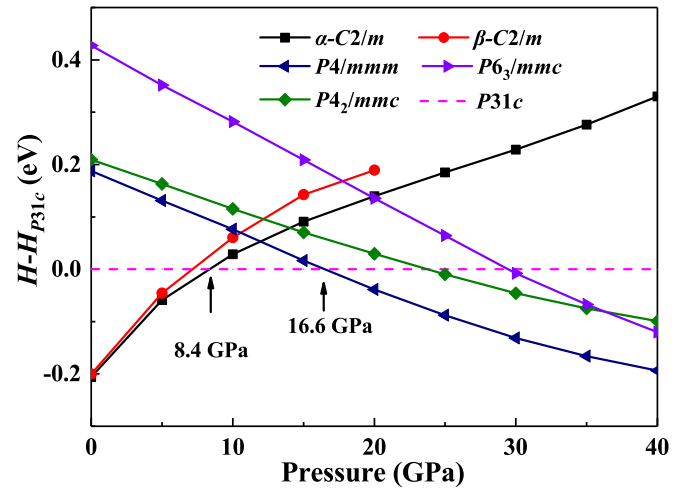
FIG. 1. Energetic stability of Bi_4I_4 as a function of pressure. Different curves show pressure evolution of the enthalpy of various Bi_4I_4 phases. The enthalpy of formation of ε-Bi_4I_4 ($P31c$) is set as the base line. Previously predicted $P4_2/mmc$ and $P6_3/mmc$ phases are also included for comparison.

$P4/mmm$, respectively. Based on optimized lattice structures, a more sophisticated and accurate Heyd-Scuseria-Ernzerhof (HSE) hybrid functional [38] was employed to calculate the electronic band structures using $4\times4\times4$ and $6\times6\times2$ Brillouin zone (BZ) meshes for the $P31c$ and $P4/mmm$ Bi_4I_4 phases, respectively. EPC calculations were performed in the framework of density-functional perturbation theory, as implemented in the QUANTUM-ESPRESSO code [39]. We adopted $4\times4\times6$ and $10\times10\times4$ k-point meshes for charge self-consistent calculations, $16\times16\times32$ and $30\times30\times12$ k-point meshes for EPC linewidth integrations, and $4\times4\times6$ and $5\times5\times2$ q-point meshes for the dynamical matrices of $P31c$ and $P4/mmm$ structures, respectively.

III. RESULTS AND DISCUSSION

A. Pressure-induced phase transitions

To search for thermodynamically stable phases of Bi_4I_4, a systematic structure prediction was carried out using CA-LYPSO methodology with up to 16 atoms per simulation cell at a series of pressure points (0, 10, 20, 30, and 50 GPa). Since the building block of Bi_4I_4 is composed of four bismuth atoms and four iodide atoms, we define the chemical formula unit (f.u.) as $[Bi_4I_4]$ when calculating relative formation enthalpy (H). The experimentally known α- and β-Bi_4I_4 were successfully reproduced, validating our methodology when applied to the current systems.

Figure 1 shows the calculated formation enthalpies of predicted high-pressure Bi_4I_4 phases compared with α- and β-Bi_4I_4. It can be seen that α-Bi_4I_4 is the ground state at ambient pressure. Two energetically favorable high-pressure phases were predicted here: a trigonal $P31c$ and a tetragonal $P4/mmm$, thereafter referred to as ε-Bi_4I_4 and ζ-Bi_4I_4, respectively. We set the enthalpy of ε-Bi_4I_4 as the baseline. It is seen that above 8.4 GPa, the ε phase becomes energetically favorable and remains stable up to 16.6 GPa, where Bi_4I_4
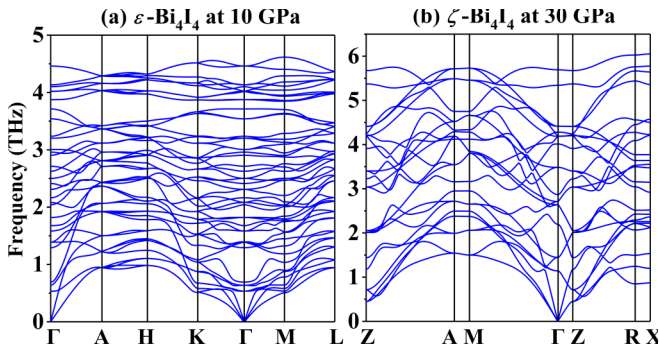
FIG. 2. Simulated phonon spectra of the newly predicted ε-Bi$_4$I$_4$ at 10 GPa (a) and ζ-Bi$_4$I$_4$ at 30 GPa (b).

transforms into the ζ phase. Simulated phonon spectra (Fig. 2) showing no imaginary phonon frequencies across the entire BZ indicate dynamical stability of the proposed ε- and ζ-Bi$_4$I$_4$ over the studied pressure range. It is noted that a very recent study proposed two other high-pressure phases ($P4_2/mmc$ and $P6_3/mmc$) for Bi$_4$I$_4$ using crystal structure prediction method based on Bayesian optimization [40]. However, these structures are energetically unfavorable compared to ε- and ζ-Bi$_4$I$_4$. Importantly, the phase transition pressure of ε-Bi$_4$I$_4$ matches well with the experimental reports when superconductivity is induced in Bi$_4$I$_4$ [20,21]. Such overlap motivates further investigation into the evolution of the structural and electronic properties of Bi$_4$I$_4$.

B. Structural evolution of Bi$_4$I$_4$

Here we present a systematic analysis of atomic arrangements and structural characteristics for Bi$_4$I$_4$ at high pressure. Figures 3(a) and 3(b) show crystal structures of the predicted ground-state α-Bi$_4$I$_4$ and metastable β-Bi$_4$I$_4$ with the identical space group $C2/m$ at ambient conditions. β-Bi$_4$I$_4$ differs from α-Bi$_4$I$_4$ merely in the stacking of its bismuth zigzag chains, while the structural unit and arrangement are similar. The structural similarities of α-Bi$_4$I$_4$ and β-Bi$_4$I$_4$ yield their nearly degenerate enthalpies, where the formation enthalpy of α-Bi$_4$I$_4$ is only 3.625 meV/atom lower than that of β-Bi$_4$I$_4$. The optimized lattice parameters and atomic coordinates of α- and β-Bi$_4$I$_4$ are listed in Table I, which are in good agreement with previously reported data [18]. We found that subtle stacking differences can affect electronic properties of Bi$_4$I$_4$ significantly, which will be discussed in subsequent sections.

The crystal structures of high-pressure phases, ε-Bi$_4$I$_4$ and ζ-Bi$_4$I$_4$, are shown in Fig. 3, with their lattice parameters and atomic positions shown in Table I. Interestingly, ε-Bi$_4$I$_4$ [Fig. 3(c)] consists of isolated I atoms and [Bi$_4$I$_3$] units indicated by the computed electron localization function (ELF) [Fig. 4(a)] [41,42]. There are two types of Bi atoms in the [Bi$_4$I$_3$] units. The inner Bi atoms (labeled as Bi$_a$) form a rather flat tetrahedron with three neighboring external Bi atoms (labeled as Bi$_b$). The vertex angle ($\angle$ Bi$_b$-Bi$_a$-Bi$_b$) is 116.4°, and the distance of the Bi-Bi bond is 3.010 Å. Each Bi$_b$ atom is connected to an I atom by a zigzag atomic bond with the nearest neighboring distance of 3.040 Å. Figure 3(d) shows the connections among these [Bi$_4$I$_3$] units. There are two types of [Bi$_4$I$_3$] units in each chain, which only differ in the internal
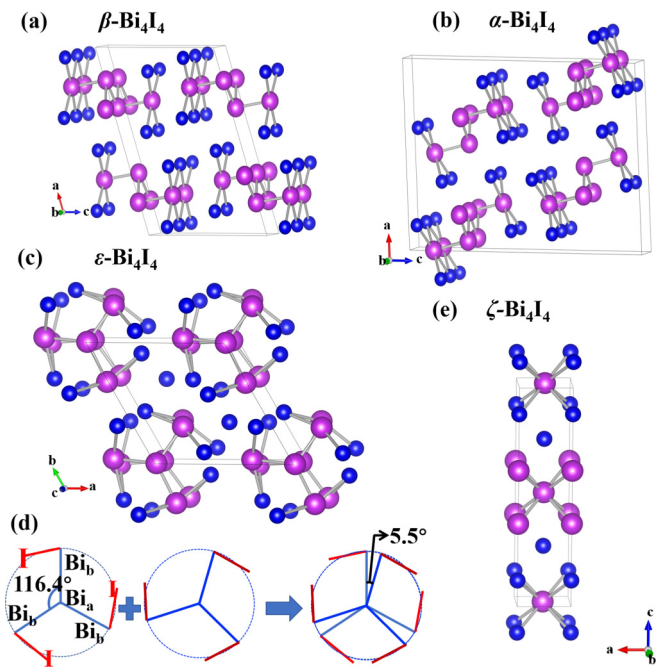
FIG. 3. Crystal structures of β-Bi$_4$I$_4$ (a) and α-Bi$_4$I$_4$ (b) with identical space group $C2/m$ viewed from the b direction, and the crystal structure of the predicted ε-Bi$_4$I$_4$ at 10 GPa (c) together with its simplified building block (d) and the crystal structure of ζ-Bi$_4$I$_4$ at 30 GPa (e). While ε-Bi$_4$I$_4$ is viewed from the c direction, ζ-Bi$_4$I$_4$ is viewed from the b direction. Bi: large purple balls; I: small blue balls.

Bi-I bonding directions. Labeling them as A and B, the chain in ε-Bi$_4$I$_4$ has the sequence ABABAB.... These units are joined together by an external Bi-I′ (the prime denotes that the I atom is from another Bi$_4$I$_3$ unit) bond with the second nearest neighboring distance between Bi and I being 3.169 Å. The remaining iodine atoms are evenly distributed in the lattice interstitial sites, with the nearest three I atoms located at an equilateral triangle position with a length of 9.249 Å (viewed in the c direction). In addition, each of these seemingly isolated iodine atoms is in average 5.617 Å away from three nearest A units and three nearest B units. The existence of nonsymmorphic symmetry (consisting of rotation and translation) in ε-Bi$_4$I$_4$ is a promising sign that topological states might be induced and protected globally even in the bulk.

The existence of these seemingly isolated iodine atoms in Fig. 3(c) is quite unusual. To further analyze how these iodine atoms interact with the neighboring (Bi$_4$I$_3$) units, we move one iodine chain along the c direction while leaving the other atoms unchanged and then calculate the static energy. It is interesting to note that the calculated enthalpy of formation has a rather high energy cost at large displacements (e.g., >5%), indicating that it is difficult for the iodine atoms to escape from the lattice, while the enthalpy surface is so smooth near the equilibrium position [Fig. 4(b)]. The underlying physical mechanism is the special structural configuration leading to the relative longer bond lengths and week interaction between the isolated iodide ions and the adjacent atoms near the equilibrium positions, which makes these ions easier to move about and creates low-frequency vibrations that benefit to the electron-phonon coupling and thus the performance of

TABLE I. Calculated lattice constants and atomic coordinates for various Bi_4I_4 phases at select pressures.

Structure	Parameter (Å,°)	Atoms	x	y	z	Pressure (GPa)
α-C2/m	$a = 14.530$	Bi1 (4i)	0.0495	0.0000	0.2538	0
	$b = 4.281$	Bi2 (4i)	0.6948	0.0000	0.2440	
	$c = 19.890$	Bi3 (4i)	1.0008	0.0000	0.1011	
	$\alpha = \gamma = 90.00$	Bi4 (4i)	0.2610	0.0000	0.6036	
	$\beta = 94.09$	I1 (4i)	0.6398	0.0000	0.0552	
		I2 (4i)	0.3612	0.0000	0.1459	
		I3 (4i)	0.1006	0.0000	0.4412	
		I4 (4i)	0.3845	0.0000	0.3648	
β-C2/m	$a = 14.758$	Bi1 (4i)	0.2103	0.0000	0.2958	0
	$b = 4.261$	Bi2 (4i)	0.8249	0.0000	0.0105	
	$c = 10.353$	I1 (4i)	0.5487	0.0000	0.2275	
	$\alpha = \gamma = 90.00$	I2 (4i)	0.8711	0.0000	0.3840	
	$\beta = 108.03$					
ε-P31c	$a = b = 9.249$	Bi1 (2a)	0.0000	0.0000	0.8812	10
	$c = 6.334$	Bi2 (6c)	0.9673	0.6650	0.7946	
	$\alpha = \beta = 90.00$	I1 (2a)	0.3333	0.6667	0.1059	
	$\gamma = 120.00$	I2 (6c)	0.8971	0.3150	0.1222	
ζ-P4/mmm	$a = b = 3.570$	Bi1 (1c)	0.5000	0.5000	0.0000	30
	$c = 14.852$	Bi2 (1d)	0.5000	0.5000	0.5000	
	$\alpha = \beta = \gamma = 90.00$	Bi3(2g)	0.0000	0.0000	0.3789	
		I1 (2h)	0.5000	0.5000	0.2548	
		I2 (2g)	0.0000	0.0000	0.8806	

superconductive properties (see more discussions below). A Bader charge analysis [43] is implemented to determine the redistributed charge value of the bismuth and iodine atoms in the entire lattice of ε-Bi_4I_4. Notably, inequivalent bismuth and

iodine atoms bear different amounts of charge according to their distinct chemical environments. The charge transferred from $(Bi_4I_3)^{\delta+}$ to $I^{\delta-}$ was determined to be $\delta = 0.4123 \, e$ at 10 GPa, illustrating the ionic nature of ε-Bi_4I_4. Such pressure-induced formation of an ionic solid in molecular systems is rare but not totally unexpected. Similar pressure-induced molecular to ionic transformation has been theoretically predicted in H_2O [44], NH_3 [45], NH_7 [30] H_2S [46], and $NH_3 \cdot H_2O$ [47] and have been experimentally verified in N_2O [48]. Our predicted ε-Bi_4I_4 to some extent resembles the partial ionicity reported in water ice [44].

Turning to ζ-Bi_4I_4 [Fig. 3(e)], the third thermodynamically stable phase at high pressure, which is energetically favorable above 16.6 GPa. According to the atomic positions listed in Table I, there are two different types of bismuth-centered cubic structures in the crystal. One consists of a body-centered Bi atom and the eight nearest I atoms with the bonding

(a) ELF of ε-Bi_4I_4 at 10 GPa

(b)
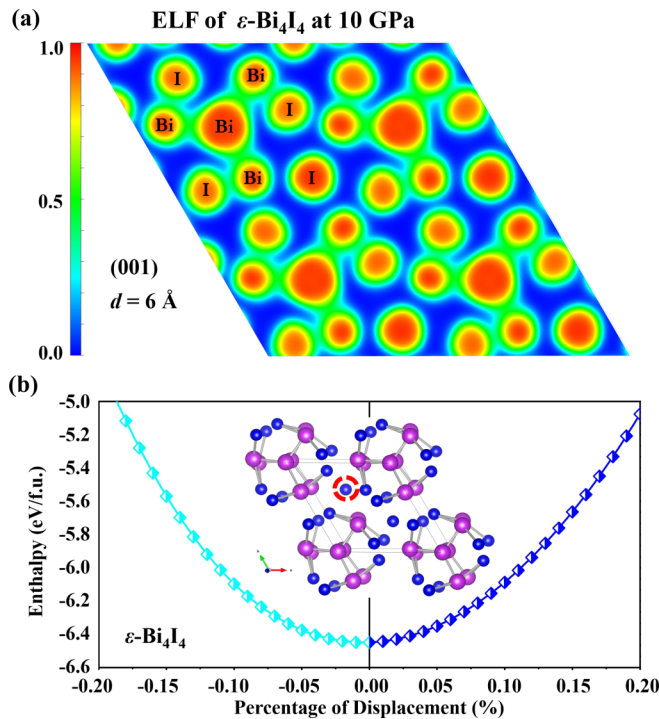
FIG. 4. Two-dimensional ELF of ε-Bi_4I_4 at 10 GPa plotted in the (001) crystalline plane (a) and the enthalpy of formation as a function of the percentage of displacement of the circled iodine atom along the c direction (b).
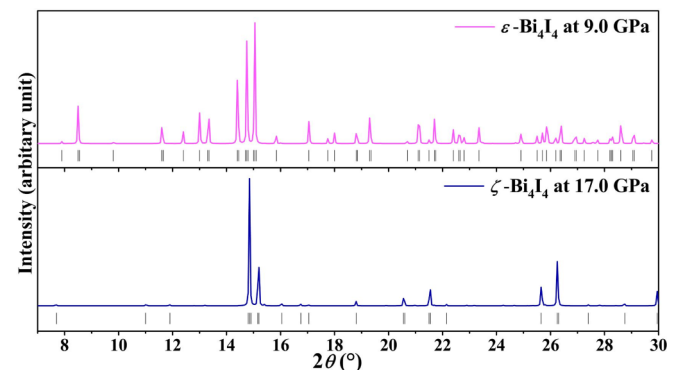
FIG. 5. The simulated synchrotron x-ray diffraction ($\lambda = 0.6888$ Å) for the high-pressure phases of Bi_4I_4 at selected pressure points.
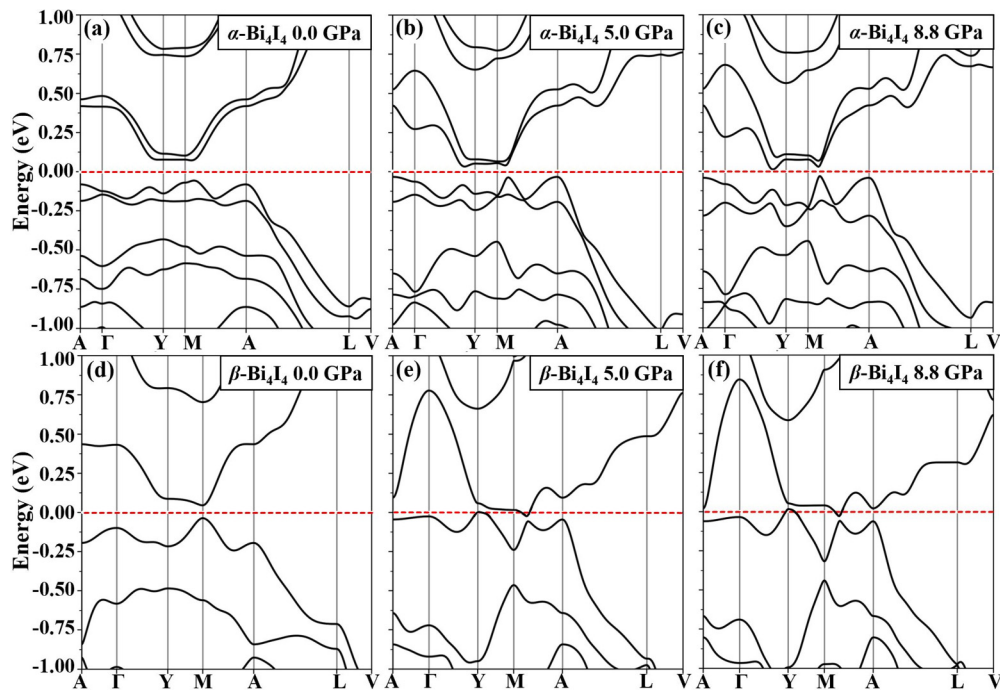
FIG. 6. Electronic band structures of α-Bi_4I_4 [(a)–(c)] and β-Bi_4I_4 [(d)–(f)] at 0.0 GPa, 5.0 GPa, and 8.8 GPa in the presence of SOC, respectively.

distance of 3.085 Å, hereby defined as X. The other is composed of purely Bi atoms, and the Bi-Bi bond is 3.100 Å in length, referred to as Y. The calculated 3D ELF of ζ-Bi_4I_4 (not shown) indicates that I_1 (2h) and I_2 (2g) do not form an actual covalent bond with the neighboring iodine and bismuth atoms. Hence, when the lattice extends, a pure-bismuth layer (Y units) is found to be corrugated due to the strong bonding abilities of the Bi 6p-orbitals. Viewing from the c direction, there are alternating layers of extended X and Y units, joined by van de Waals forces originating from the intervening pure iodine layers. Such repeated units of XIYI along the c direction will finally turn ζ-Bi_4I_4 into a quasi-3D structural component. These newly predicted high-pressure ε-Bi_4I_4 and ζ-Bi_4I_4 phases differ considerably from the known $C2/m$ Bi_4I_4, which leads to distinct behaviors of Bi_4I_4 under high pressures. As no *in situ* experimental XRD patterns are available for comparison with the current structural candidates, we hereby provide the simulated XRD pattern of ε-Bi_4I_4 and ζ-Bi_4I_4 in Fig. 5 for future experimental comparison. Below we discuss the evolution of the electronic properties of Bi_4I_4.

C. Evolution of electronic properties of Bi_4I_4

To investigate the effect of external pressure on the electronic properties, we show in Fig. 6 and Fig. 7 the evolution of electronic band structures for the high-pressure phases of Bi_4I_4. As previously mentioned, $C2/m$ Bi_4I_4 has two polymorphs (α-Bi_4I_4 and β-Bi_4I_4) within the low-pressure range, where the different stacking modes of their molecular chains lead to diverging electronic properties. The evolution of band structures with increasing hydrostatic pressure for the trivial insulator α-Bi_4I_4 and the nontrivial topological insulator β-Bi_4I_4 at DFT level are plotted. Because of the

symmetry requirements, a crossing of the conduction minimum and valence maximum at M point is forbidden in β-Bi_4I_4, and, consequently, they strongly repel each other under high pressure with the gap further opened up to 0.375 eV at 8.8 GPa. While, the valence and conduction energy bands crossing the Fermi level in the Y point and the middle of the M-A direction gradually give rise to small hole and electron pockets and turns metallic. It can be seen that α-Bi_4I_4 remains insulating with increasing external pressure at least till the phase boundary of 8.8 GPa.

Figure 7 shows simulated band structures of ε-Bi_4I_4 and ζ-Bi_4I_4 at various selected pressure points. It can be inferred that ε-Bi_4I_4 and ζ-Bi_4I_4 are both metallic phases, as there are several energy bands crossing the Fermi level. Moreover, the nonsymmorphic symmetry of ε-Bi_4I_4 induces band crossing in the bulk band. There exhibit several Dirac-cone type dispersions near the Fermi energy. Note that these band crossings are not pinned to either the origin or the boundary of BZ, and the nonsymmorphic symmetry of ε-Bi_4I_4 belongs to the unitary type, which would require the system to be in a topological semimetal phase [49]. Considering that bismuth belongs to the family of heavy metal elements, the SOC effect is taken into account and a more accurate calculation method, the HSE hybrid functional method, is employed here. As shown in Figs. 7(a)–7(c), the energy gap for ε-Bi_4I_4 intersecting along the Γ-A-H path remains gapless, while that near the L point stays gapped within the pressure range, which suggests that ε-Bi_4I_4 may contain coexisting topological semimetal and topological features. The fourfold degeneracy at the A point in the BZ is locally protected by the nonsymmorphic symmetry even if the crossing point is lowered at increasing pressure. Further study may reveal additional interesting behaviors, e.g., contrasting local and global topologies.
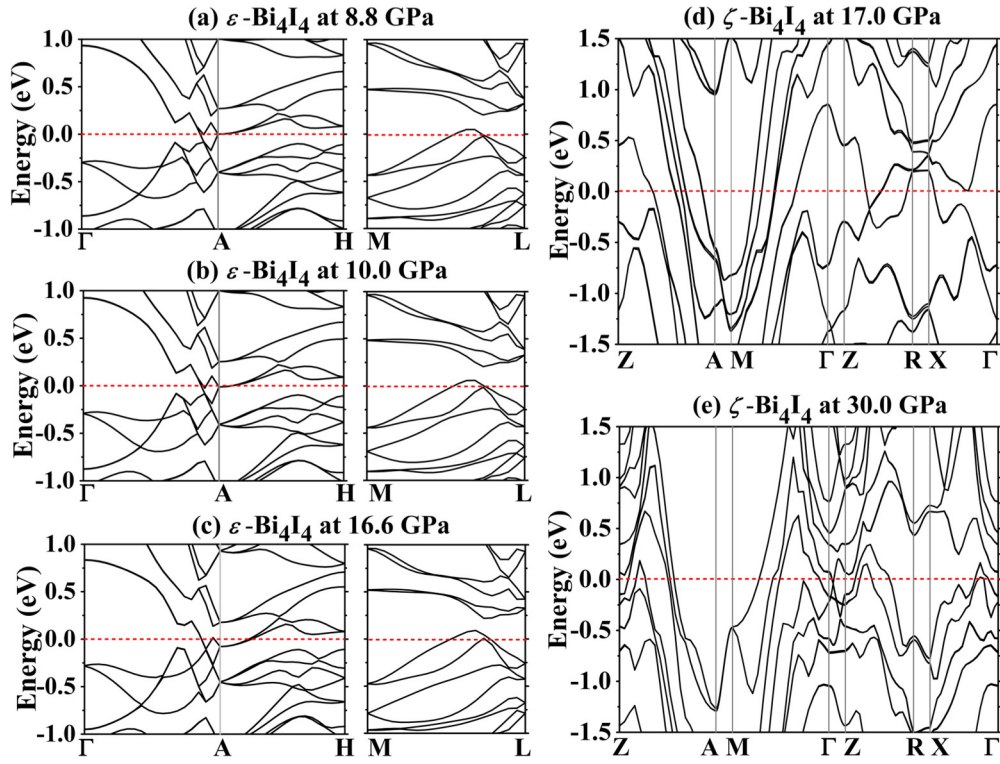
FIG. 7. Electronic band structures of ε-Bi$_4$I$_4$ and ζ-Bi$_4$I$_4$ with SOC included and using the HSE hybrid functional for (a)–(c) ε-Bi$_4$I$_4$ along the Γ-A-H, M-L path and [(d) and (e)] ζ-Bi$_4$I$_4$ in the entire BZ. The red line indicates the Fermi level.

D. Pressure-induced superconductivity of Bi$_4$I$_4$

To understand the pressure-induced superconductivity of Bi$_4$I$_4$, we have performed systematic EPC calculations. Figure 8 presents the simulated partial phonon density of states, Eliashberg spectral functions $\alpha^2F(\omega)$, and integrated EPC constant $\lambda(\omega)$ of ε-Bi$_4$I$_4$ at 15 GPa and ζ-Bi$_4$I$_4$ at 30 GPa. The EPC constants λ are 0.67 and 0.61 for ε-Bi$_4$I$_4$ and ζ-Bi$_4$I$_4$, respectively. For ε-Bi$_4$I$_4$, 44.3% of the total λ comes from the low frequency Bi vibrations, while high-frequency I vibrations and intermediate Bi-I modes contribute almost equally to total λ at 28.2% and 27.5%, respectively. Differently, for ζ-Bi$_4$I$_4$, intermediate Bi-I modes have the largest contribution of 49.6%, followed by Bi vibrations of 38.5%, and I vibrations only contribute 11.9% of the total λ.

The superconducting critical temperature (T_c) of Bi$_4$I$_4$ at high pressures is estimated using Allen-Dynes modified McMillian equation [50]:

$$T_c = \frac{\omega_{\log}}{1.2} \exp \left\{ -\frac{1.04(1+\lambda)}{[\lambda - \mu^*(1+0.62\lambda)]} \right\},$$

where the Coulomb pseudopotential μ^* is set to a typical value of 0.1. The predicted T_c is shown as a function of pressure in Fig. 9. The calculated T_c is 3.3 K for ε phase at 9 GPa, which is slightly reduced to 3.0 K at 13 GPa and remains the same to 16 GPa. Under further compression, T_c first increases to 4.0 K and then decreases as pressure increases. The change of T_c can be well correlated to the high-pressure behavior of λ. Results in the inset of Fig. 9 clearly show that both T_c and λ share a similar trend under compression in spite of

the increased $\omega_{\log}$. Within each high-pressure phase, λ always decreases as pressure is increased, resulting in a reduced T_c. This is because the partial coupling strengths λ_{qv} is in inverse proportion to ω_{qv}. By increasing the pressure, the bond lengths between atoms are shortened and, thus, the phonon frequency ω_{qv} is increased, leading to the decreased λ_{qv}. The increase of T_c around 16 GPa is attributed to the phase transformation of Bi$_4$I$_4$ from ε phase to ζ phase as we can see a sudden increase of λ around the transition pressure point. Although λ at 18 GPa is very close to λ at 9 GPa around 0.72, $\omega_{\log}$ is slightly increased from 86.6 K at 9 GPa to 97.5 K at 18 GPa that results in an enhanced T_c. Overall, the predicted T_c agrees well with the experimental measurements [20,21], especially the results reported by Pisoni and coworkers [21]. Importantly, both experiments show the similar pressure-induced increase then decrease behavior of T_c that might be related to our proposed second high-pressure phase transition. It is noted that the turning point of T_c reported by Qi and coworkers [20] is slightly higher than our predicted pressure and that in Ref. [21]. This may be caused by the hinderance of phase transformation from ε phase to ζ phase by kinetic barriers in their experiments, which allowed the increase of T_c in the ε phase to last over a larger pressure range, resulting in higher transition temperatures and a later turning pressure point. Admittedly, the amorphization tendency proposed previously also provides a possible scenario for the experimental measurement. Since there have been no *in situ* crystalline characterization measurements for this fascinating material so far, further efforts are still needed to explore the origin of the observed superconductivity.
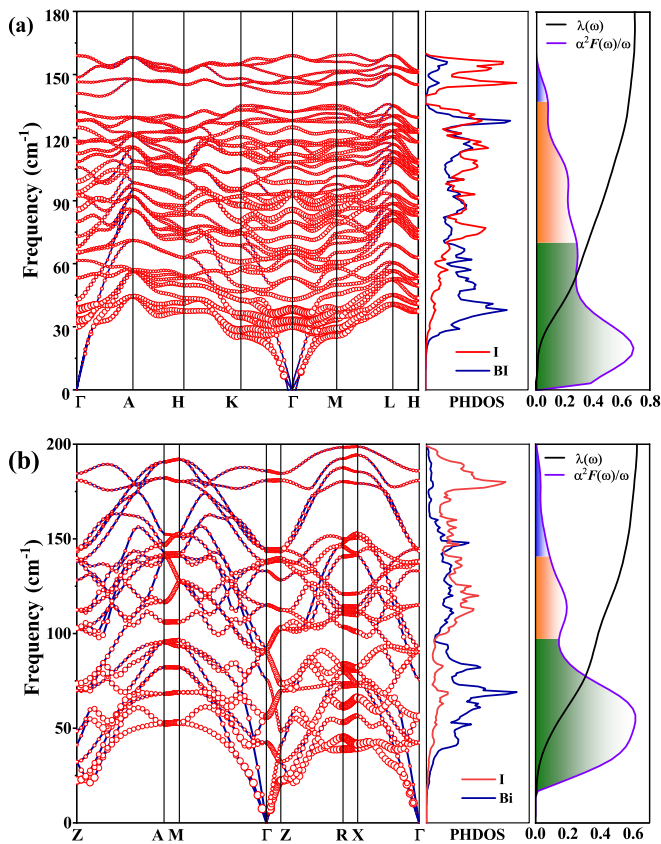
FIG. 8. The calculated phonon dispersion, partial phonon density of states, Eliashberg spectral functions $\alpha^2 F(\omega)$, and integrated EPC constant $\lambda(\omega)$ for (a) ε-Bi$_4$I$_4$ at 10 GPa and (b) ζ-Bi$_4$I$_4$ at 30 GPa. The size of the red circles of the phonon spectra indicates the strength of the partial EPC constant λ_{qv}.

FIG. 9. Pressure dependence of theoretically predicted T_c for ε-Bi$_4$I$_4$ and ζ-Bi$_4$I$_4$ compared to experimentally measured T_c.

IV. CONCLUSIONS

Employing a systematic structure search approach combined with first-principles calculations, we have identified two high-pressure bismuth iodide phases, namely the ε-Bi$_4$I$_4$ phase in $P31c$ symmetry and the ζ-Bi$_4$I$_4$ phase in $P4/mmm$ symmetry, apart from the known ambient-pressure phases. The ε-Bi$_4$I$_4$ phase is stable from 8.4 to 16.6 GPa, while the ζ-Bi$_4$I$_4$ phase is energetically favorable above 16.6 GPa. The phase transition point well matches the recently observed abrupt pressure-induced electrical property changes in β-Bi$_4$I$_4$ and a subsequent emergence of metallization of the system. The divergent response of energy gap to external pressure in ambient pressure phases, α- and β-Bi$_4$I$_4$, stems from their slightly different staking modes. The topological

state in β-Bi$_4$I$_4$ is strengthened by pressure. An interesting ionic nature with the formation of $(Bi_4I_3)^{\delta+}$ and $I^{\delta-}$ units in its crystal structure ($\delta = 0.4123\ e$) may explain the previously measured sudden drop of electrical resistivity in Bi$_4$I$_4$. The metallicity increases with rising pressure while a structural transition occurs leading to another high-pressure phase ζ-Bi$_4$I$_4$. High-pressure superconductivity of ε- and ζ-Bi$_4$I$_4$ is confirmed by EPC calculations, where the estimated T_c agree well with experimental measurements. Our present findings provide additional insights for understanding the pressure-induced superconductivity in Bi$_4$I$_4$. These results are expected to stimulate further theoretical and experimental exploration on the coexistence of topological states with superconductivity in the current and similar low-dimensional materials.

[1] J. Alicea and A. Stern, Phys. Scr. **2015**, 014006 (2015).

[2] C. L. Kane and E. J. Mele, Phys. Rev. Lett. **95**, 226801 (2005).

[3] J. E. Moore and L. Balents, Phys. Rev. B **75**, 121306(R) (2007).

[4] B. A. Bernevig, T. L. Hughes, and S.-C. Zhang, Science **314**, 1757 (2006).

[5] B. A. Bernevig and S.-C. Zhang, Phys. Rev. Lett. **96**, 106802 (2006).

[6] L. Fu and C. L. Kane, Phys. Rev. B **76**, 045302 (2007).

[7] D. Hsieh, D. Qian, L. Wray, Y. Xia, Y. S. Hor, R. J. Cava, and M. Z. Hasan, Nature **452**, 970 (2008).

[8] S.-M. Huang, S.-Y. Xu, I. Belopolski, C.-C. Lee, G. Chang, B. Wang, N. Alidoust, G. Bian, M. Neupane, C. Zhang et al., Nat. Commun. **6**, 7373 (2015).

[9] L. Fu, C. L. Kane, and E. J. Mele, Phys. Rev. Lett. **98**, 106803 (2007).

[10] Z. Ringel, Y. E. Kraus, and A. Stern, Phys. Rev. B **86**, 045102 (2012).

[11] E. J. Mele, Phys. Scr. **2015**, 014004 (2015).

[12] G. Autès, A. Isaeva, L. Moreschini, J. C. Johannsen, A. Pisoni, R. Mori, W. Zhang, T. G. Filatova, A. N. Kuznetsov, L. Forró *et al.*, Nat. Mater. **15**, 154 (2016).

[13] C.-C. Liu, J.-J. Zhou, Y. Yao, and F. Zhang, Phys. Rev. Lett. **116**, 066801 (2016).

[14] R. Noguchi, T. Takahashi, K. Kuroda, M. Ochi, T. Shirasawa, M. Sakano, C. Bareille, M. Nakayama, M. D. Watson, K. Yaji, and A. Harasawa, Nature **566**, 518 (2019).

[15] P. De Marcillac, N. Coron, G. Dambier, J. Leblanc, and J.-P. Moalic, Nature **422**, 876 (2003).

[16] M. Z. Hasan, S.-Y. Xu, and G. Bian, Phys. Scr. **2015**, 014001 (2015).

[17] O. V. Yazyev, E. Kioupakis, J. E. Moore, and S. G. Louie, Phys. Rev. B **85**, 161101(R) (2012).

[18] H. G. von Schnering, H. von Benda, and C. Kalveram, Z. Anorg. Allg. Chem. **438**, 37 (1978).

[19] T. Filatova, P. Gurin, L. Kloo, V. Kulbachinskii, A. Kuznetsov, V. Kytin, M. Lindsjo, and B. Popovkin, J. Solid State Chem. **180**, 1103 (2007).

[20] Y. Qi, W. Shi, P. Werner, P. G. Naumov, W. Schnelle, L. Wang, K. G. Rana, S. Parkin, S. A. Medvedev, B. Yan, and C. Felser, npj Quant. Mater. **3**, 4 (2018).

[21] A. Pisoni, R. Gaál, A. Zeugner, V. Falkowski, A. Isaeva, H. Huppertz, G. Autès, O. V. Yazyev, and L. Forró, Phys. Rev. B **95**, 235149 (2017).

[22] L. Fu and C. L. Kane, Phys. Rev. Lett. **100**, 096407 (2008).

[23] X. L. Qi, T. L. Hughes, S. Raghu, and S. C. Zhang, Phys. Rev. Lett. **102**, 187001 (2009).

[24] Y. Wang, J. Lv, L. Zhu, and Y. Ma, Phys. Rev. B **82**, 094116 (2010).

[25] Y. Wang, J. Lv, L. Zhu, and Y. Ma, Comput. Phys. Commun. **183**, 2063 (2012).

[26] X. Zhang, Y. Wang, J. Lv, C. Zhu, Q. Li, M. Zhang, Q. Li, and Y. Ma, J. Chem. Phys. **138**, 114101 (2013).

[27] Q. Li, D. Zhou, W. Zheng, Y. Ma, and C. Chen, Phys. Rev. Lett. **110**, 136403 (2013).

[28] M. Zhang, H. Liu, Q. Li, B. Gao, Y. Wang, H. Li, C. Chen, and Y. Ma, Phys. Rev. Lett. **114**, 015502 (2015).

[29] J. Zhang, J. Lv, H. Li, X. Feng, C. Lu, S. A. T. Redfern, H. Liu, C. Chen, and Y. Ma, Phys. Rev. Lett. **121**, 255703 (2018).

[30] X. Song, K. Yin, Y. Wang, A. Hermann, H. Liu, J. Lv, Q. Li, C. Chen, and Y. Ma, J. Phys. Chem. Lett. **10**, 2761 (2019).

[31] D. Zhou, Q. Li, W. Zheng, Y. Ma, and C. Chen, Phys. Chem. Chem. Phys. **19**, 4560 (2017).

[32] G. Kresse and J. Furthmüller, Phys. Rev. B **54**, 11169 (1996).

[33] J. P. Perdew, K. Burke, and M. Ernzerhof, Phys. Rev. Lett. **77**, 3865 (1996).

[34] P. E. Blöchl, Phys. Rev. B **50**, 17953 (1994).

[35] H. J. Monkhorst, Phys. Rev. B **13**, 5188 (1976).

[36] S. Grimme, J. Antony, S. Ehrlich, and H. Krieg, J. Chem. Phys. **132**, 154104 (2010).

[37] A. Togo, F. Oba, and I. Tanaka, Phys. Rev. B **78**, 134106 (2008).

[38] J. Heyd, G. E. Scuseria, and M. Ernzerhof, J. Chem. Phys. **118**, 8207 (2003).

[39] P. Giannozzi, S. Baroni, N. Bonini, M. Calandra, R. Car, C. Cavazzoni, D. Ceresoli, G. L. Chiarotti, M. Cococcioni, I. Dabo *et al.*, J. Phys.: Condens. Matter **21**, 395502 (2009).

[40] X. Wang, J. Wu, J. Wang, T. Chen, H. Gao, P. Lu, Q. Chen, C. Ding, J. Wen, and J. Sun, Phys. Rev. B **98**, 174112 (2018).

[41] A. Savin, O. Jepsen, J. Flad, O. K. Andersen, H. Preuss, and H. G. von Schnering, Angew. Chem. Int. Edit. **31**, 187 (1992).

[42] A. D. Becke and K. E. Edgecombe, J. Chem. Phys. **92**, 5397 (1990).

[43] R. F. Bader, Acc. Chem. Res. **18**, 9 (1985).

[44] Y. Wang, H. Liu, J. Lv, L. Zhu, H. Wang, and Y. Ma, Nat. Commun. **2**, 563 (2011).

[45] C. J. Pickard and R. Needs, Nat. Mater. **7**, 775 (2008).

[46] R. Rousseau, M. Boero, M. Bernasconi, M. Parrinello, and K. Terakura, Phys. Rev. Lett. **85**, 1254 (2000).

[47] A. D. Fortes, J. P. Brodholt, I. G. Wood, L. Vočadlo, and H. Jenkins, J. Chem. Phys. **115**, 7006 (2001).

[48] M. Somayazulu, A. Madduri, A. F. Goncharov, O. Tschauner, P. F. McMillan, H.-K. Mao, and R. J. Hemley, Phys. Rev. Lett. **87**, 135504 (2001).

[49] Y. X. Zhao and A. P. Schnyder, Phys. Rev. B **94**, 195109 (2016).

[50] P. B. Allen and R. C. Dynes, Phys. Rev. B **12**, 905 (1975).